Engineering Failure Analysis 159 (2024) 108092

Contents lists available at ScienceDirect

Engineering Failure Analysis

journal homepage: www.elsevier.com/locate/engfailanal

Thermal treatment effects on rock fracture behaviour under three loading modes: A comparative analysis of granite and mudstone

Abdel Kareem Alzo'ubi [a], Mahmoud Alneasan [b,*], Farid Ibrahim [c], Nader M. Okasha [a], Masoomeh Mirrashid [d]

[a] Civil Engineering Department, Abu Dhabi University, Al Ain, United Arab Emirates
[b] Civil Engineering Department, Tishreen University, Latakia, Syria
[c] Computer Science & IT Department, Abu Dhabi University, Al Ain, United Arab Emirates
[d] Research Assistant at the Civil Engineering Department, Abu Dhabi University, United Arab Emirates

ARTICLE INFO

Keywords:
Thermal treatment
Rock fracture behaviour
Fracture criteria
Fracture process zone
mixed mode loading I/II

ABSTRACT

Temperature and thermal damage have a major impact on the behaviour of fractures in the earth's crust. For deep earth engineering such as underground coal gasification, geothermal energy extraction, and nuclear waste repositories, developing fracture criteria governing the propagation of fractures under thermal effect is crucial. As a result, the ability of stress, energy, and strain-based fracture criteria to predict rock fracture behavior both before and after thermal treatment is assessed in this paper considering two rock types; granite, and mudstone, which are very different from one another in terms of their mineralogical composition and mechanical properties. The overall findings showed that the energy-based criterion was more effective in predicting fracture parameters both before and after thermal treatment than the stress and strain-based criteria. Specifically, after thermal treatment at 500 °C for the granite, and at any temperature for the mudstone, the strain-based criterion was no longer valid. It was found that the temperature and loading mode have a significant impact on the granite's transition from brittle to ductile, where this transition can occur at an approximated temperature of 460 °C. Meanwhile, an increase in brittleness with rising temperature was noted in mudstone. Moreover, the Fracture Process Zone (FPZ) size was predicted by the energy-based criterion to be greater than that predicted by stress and strain-based criteria. It was found that the FPZ size is proportional to the brittleness degree of the two rock types, which is considerably impacted by thermal treatment. In addition, this study discusses several critical areas in rock fracture mechanics in the presence of thermal effects including fracture envelopes under mixed mode loading I/II, fracture stress, and initial crack extension angle. All of these are of high importance in assessing the safety and stability of rock structures in the presence of thermal effects.

1. Introduction

Temperature is one of the most significant factors that threaten the safety and stability of rock structures as deep earth engineering advances [1–3]. Therefore, determining the models governing the behaviour of fractures in rock masses enhances the understanding of

* Corresponding author.
E-mail addresses: abdel.alzoubi@adu.ac.ae (A. Kareem Alzo'ubi), mahmoud.alneasan@tishreen.edu.sy (M. Alneasan), farid.ibrahim@adu.ac.ae (F. Ibrahim), nader.okasha@adu.ac.ae (N.M. Okasha), mirrashid.research@adu.ac.ae (M. Mirrashid).

https://doi.org/10.1016/j.engfailanal.2024.108092
Received 30 November 2023; Received in revised form 19 January 2024; Accepted 4 February 2024
Available online 15 February 2024
1350-6307/

the effect of temperature on these fractures, and the potential for predicting their initiation, propagation, and coalescence to form continuous rupture surfaces. Due to the large spread of fractures in the earth's crust, Linear Elastic Fracture Mechanics (LEFM) has received widespread attention from scholars in the fields of rock mechanics, geology, geophysics, mining, and civil engineering [4–8]. To describe fracture behaviour under different loading modes, many facture criteria have been developed in LEFM. These criteria can primarily be divided into stress, energy, and strain-based criteria. In terms of practical applications, the maximum tangential stress, which is a stress-based criterion (σ-criterion) [9], the minimum strain energy density, which is an energy-based criterion (S-criterion) [10], and the maximum tangential strain, which is a strain-based criterion (ε-criterion) [11] are the most widely employed in rock fracture mechanics. By taking into account the role of *T-stress* in the fracture process, the three previously mentioned criteria -known as the conventional fracture criteria- became the generalized fracture criteria. In terms of rock mechanics, taking into consideration the contribution of *T-stress* to the fracture process is extremely important since it enables generalized fracture criteria to take the size of the Fracture Process Zone (FPZ) into account [12].

Many experts in rock mechanics and geological engineering are interested in studying the effect of temperature on the safety and stability of fractured rocks. Most studies [13–17] focused on the impact of temperature on pure mode I fracture behaviour. However, because fractures in the Earth's crust can develop under different loading conditions, and because the pure mode I test does not allow alone for the development of a comprehensive analytical model to describe the behaviour of these fractures in rock masses; some scholars have focused on assessing the thermal effect on mixed mode I/II fracture behaviour in various rock types. Wu, et al. [18] studied the mixed mode I/II fracture characteristics of thermal treated granite based on the extended finite element method by considering the cohesive zone model (CZM) and concluded that the numerical model can successfully predict the fracture stress and fracture trajectory within a temperature range of 25 °C to 600 °C. Feng, et al. [19] investigated fracture behaviour in the sandstone under mixed mode loading I/II after thermal treatment at temperatures between 20 °C and 600 °C and concluded a sharp decrease in the fracture toughness after thermal treatment at 500 °C. Kang, et al. [20] concluded a decline in the fracture toughness of granite under all loading modes with a temperature increase from 20 °C to 900 °C, and demonstrated the ability of the generalized maximum tangential stress criterion to predict fracture parameters under thermal effect. Yin, et al. [21] investigated mixed mode I/II tensile fracture of thermally treated notched Brazilian disks of granite at temperatures between 25 °C and 800 °C. They concluded that the temperature can greatly affect the mixed mode fracture toughness and the brittleness of the granite, but the crack extension angle was not sensitive to high temperature. In addition, they found that the fracture of thermally treated granite obeys a stress-based fracture criterion rather than a strain-based criterion. Moreover, the effect of thermal cycling on the mechanical behaviour of granite at temperatures between 20 °C and 300 °C was studied by Feng, et al. [22]. They found that thermal cycling promotes the growth of crack networks and deteriorates the mechanical stability of granite. They also found that the generalized maximum tangential stress criterion predictions were in high agreement with the experimental data. Feng, et al. [23] investigated the mixed mode I/II fracture behaviour of sandstone after thermal treatment at three temperatures of 25, 350, and 700 °C and found approximately linear increase in the fracture process zone with temperature. Suo, et al. [24] demonstrated the ability of the generalized maximum tangential stress criterion to predict fracture parameters in SCB specimens of shale under different loading modes and temperatures. Wei, et al. [25] investigated the effect of specimen geometry on mode I, II, and mixed mode I/II rock fracture toughness using the generalized maximum tangential strain criterion and concluded that this criterion can provide better estimates for the experimental results than other frequently-used fracture criteria.

Since each of the previous studies was conducted under mixed mode loading I/II, focused on a single type of rock, and as researchers relied on the stress-based criterion to predict fracture parameters, this field needs to be further explored and more research is required to determine the ability of the generalized fracture criteria to predict rock fracture behaviour after thermal treatment. Accordingly, two rock types that are radically distinct in mineralogical composition and mechanical behaviour were investigated in this study to evaluate the ability of the stress, energy, and strain-based fracture criteria to predict rock fracture behaviour before and after thermal treatment under various loading modes. The studied rocks included granite and mudstone, and the fracture criteria included the generalized maximum tangential stress criterion (Gσ-criterion) of Smith, et al. [26], the generalized minimum strain energy density criterion (GS-criterion) of Ayatollahi, et al. [27], and the generalized maximum tangential strain criterion (Gε-criterion) of Mirsayar [28].

2. Theoretical background of fracture criteria

Fracture criteria are a very important concept in the study of rock fracture mechanics that can be used to predict conditions under which a crack can initiate and propagate in a rock mass (field scale) [6,29,30] or rock sample (laboratory scale) [4,31–33]. They can make accurate predictions about fracture envelopes, fracture stress, initial crack extension angle, and FPZ size [34]. Conventional fracture criteria take the singular terms of William's [35] stress distribution functions into account (the first two terms in Equation (1)). Stress and strain fields and fracture parameters can be predicted with greater accuracy by including non-singular terms (the third and fourth terms in Equation (1)). The fracture criteria that use these terms are known as generalized fracture criteria. In generalized fracture criteria, the contribution of the higher-order term $O\sqrt{r}$ vanishes in the vicinity of the crack tip, leaving only the effect of the third term. The third term is the *T-stress* term, which is independent of the radial distance from the crack tip (r) and is mainly influenced by the geometry and loading configurations.

$$\begin{bmatrix}\sigma_{rr}\\ \sigma_{\theta\theta}\\ \sigma_{r\theta}\end{bmatrix} = \overbrace{\frac{K_I}{\sqrt{2\pi r}}\begin{bmatrix} cos\frac{\theta}{2}\left(1+sin^2\frac{\theta}{2}\right)\\ cos^3\frac{\theta}{2}\\ sin\frac{\theta}{2}cos^2\frac{\theta}{2}\end{bmatrix} + \frac{K_{II}}{\sqrt{2\pi r}}\begin{bmatrix} sin\frac{\theta}{2}\left(1-3sin^2\frac{\theta}{2}\right)\\ -3sin\frac{\theta}{2}cos^2\frac{\theta}{2}\\ cos\frac{\theta}{2}\left(1-3sin^2\frac{\theta}{2}\right)\end{bmatrix}}^{\text{Conventional fracutre criteria } (\sigma, \text{ S and } \varepsilon-\text{criteria})} \underbrace{+T\begin{bmatrix}cos^2\theta\\ sin^2\theta\\ -sin\theta cos\theta\end{bmatrix} + O\sqrt{r}}_{} \quad (1)$$

Generalized fracture criteria ($G\sigma$, GS and $G\varepsilon-$criteria)

where σ_{rr}, $\sigma_{\theta\theta}$ and $\sigma_{r\theta}$ in Equation (1) are the radial, tangential, and shear stresses in polar coordinates around the crack tip. K_I and K_{II} are modes I and II stress intensity factors, respectively, r is the radial distance from the crack tip, and θ is the angle between the main plane of the pre-existing crack and the new crack.

2.1. Generalized maximum tangential stress criterion (Gσ-criterion)

The second row of Equation (1) depicts the generalized form of tangential stress $\sigma_{\theta\theta}$ around the crack tip for any homogeneous and isotropic body under mixed mode loading I/II. As previously indicated, the higher order term $O\sqrt{r}$ can be ignored near the crack tip, and thus $\sigma_{\theta\theta}$ becomes [26]:

$$\sigma_{\theta\theta} = \frac{1}{\sqrt{2\pi r}}cos\frac{\theta}{2}\left[K_I cos^2\frac{\theta}{2} - \frac{3}{2}K_{II}sin\theta\right] + Tsin^2\theta \quad (2)$$

Based on this criterion, a pre-existing crack in a brittle material can grow when the maximum tangential stress $\sigma_{\theta\theta}^{max}$ reaches the critical value of the material strength σ_c at a critical radius r_c in front of the crack tip. The term r_c in rock mechanics can be referred to as the radius of the fracture process zone (FPZ). The new crack's path is perpendicular to $\sigma_{\theta\theta}^{max}$ and forms an angle θ_m with the main plane of a pre-existing crack. The angle θ_m can be found using:

$$\frac{\partial\sigma_{\theta\theta}}{\partial\theta} = 0.0 \leftrightarrow \theta = \theta_m \& r = r_c \quad (3)$$

$$\frac{\partial\sigma_{\theta\theta}}{\partial\theta} = 0.0 \rightarrow K_I sin\theta_m + K_{II}(3cos\theta_m - 1) - \gamma sin\frac{\theta_m}{2}cos\theta_m = 0.0 \quad (4)$$

where $\gamma = \frac{16}{3}T\sqrt{2\pi r_c}$.In general, the critical distance from the crack tip r_c is shown in a non-dimensional form of $\alpha = \sqrt{\frac{2r_c}{a}}$, where ($a$) is the half-length of the pre-existing crack. Accordingly, the parameter γ is a function of the biaxiality ratio B and the effective stress intensity factor K_{eff} as shown in Equation (5), where the biaxiality ratio is the ratio of *T-stress* relative to the effective stress intensity factor.

$$\gamma = \frac{16}{3}B\alpha K_{eff}, K_{eff} = \sqrt{K_I^2 + K_{II}^2}, B = \frac{T\sqrt{\pi a}}{K_{eff}} \quad (5)$$

By calculating the crack extension angle θ_m from Equation (4) and substituting it in Equation (2), the general equation of the Gσ-criterion for crack growth under mixed mode loading I/II can be obtained as follows:

$$cos\frac{\theta_m}{2}\left[K_I cos^2\frac{\theta_m}{2} - \frac{3}{2}K_{II}sin\theta_m\right] + B\alpha K_{eff}sin^2\theta_m - K_{IC} = 0.0 \quad (6)$$

Consequently, the fracture envelope under mixed mode loading can be predicted by the fracture resistance ratios K_I/K_{IC} and K_{II}/K_{IC} extracted from Equation (6) as follows:

$$\frac{K_I}{K_{IC}} = \left[cos^3\frac{\theta_m}{2} - 3Msin\frac{\theta_m}{2}cos^2\frac{\theta_m}{2} + B\alpha\sqrt{1+M^2}\,sin^2\theta_m\right]^{-1} \quad (7)$$

$$\frac{K_{II}}{K_{IC}} = \left[M^{-1}cos^3\frac{\theta_m}{2} - 3sin\frac{\theta_m}{2}cos^2\frac{\theta_m}{2} + B\alpha\sqrt{1+M^{-2}}\,sin^2\theta_m\right]^{-1} \quad (8)$$

where $M = K_{II}/K_I$ is the mode mixity ratio that depends on the geometry of the problem.

Fracture stress $\sigma^f_{I/II}$ under mixed mode loading can be deduced from Equation (6) by substituting stress intensity factors $K_I = \sigma\sqrt{\pi a}K^I_{dim}$ and $K_{II} = \sigma\sqrt{\pi a}K^{II}_{dim}$ in this equation. Since K^I_{dim} and K^{II}_{dim} are dimensionless stress intensity factors and they are fundamentally a function of the geometry of the rock sample. Consequently, the dimensionless fracture stress $\sigma^f_{dim} = \sigma^f_{I/II} / \sigma^f_I$ can be expressed as follows:

$$\sigma^f_{DIM} = \frac{K^I_{dim}}{K^I_{dim}cos^3\frac{\theta_m}{2} - 3K^{II}_{dim}sin\frac{\theta_m}{2}cos^2\frac{\theta_m}{2} + B\alpha\sqrt{{K^I_{dim}}^2 + {K^{II}_{dim}}^2 sin^2\theta_m}} \tag{9}$$

2.2. Generalized minimum strain energy density criterion (GS-criterion)

According to this criterion, a pre-existing crack in a brittle material can grow when the minimum strain energy density $S^{min}_{\theta\theta}$, reaches the critical value of material strength, S_c, at a critical radius, r_c, in front of the crack tip. The direction of the new crack is in the direction of $S^{min}_{\theta\theta}$ and it makes an angle θ_m with the main plane of the pre-existing crack. Equation (10) illustrates the general form of the strain energy density, while the angle θ_m can be found following the conditions shown in this equation [27]:

$$S = \frac{1}{2G}\left[\frac{k+1}{8}(\sigma_{rr} + \sigma_{\theta\theta})^2 - \sigma_{rr}\sigma_{\theta\theta} + {\sigma_{r\theta}}^2\right] = A_1K_I^2 + A_2K_{II}^2 + 2A_3K_IK_{II} + 2A_4\sqrt{2\pi r}K_IT + 2A_5\sqrt{2\pi r}K_{II}T + A_6(2\pi r)T^2, \tag{10}$$

$$\left.\frac{\partial S}{\partial \theta}\right|_{\theta=\theta_m} = 0.0 \text{ and } \left.\frac{\partial^2 S}{\partial \theta^2}\right|_{\theta=\theta_m} > 0.0$$

where A_1 to A_6 are shown in Appendix I, G is the shear modulus, $k = 3\text{-}4\nu$ for plane strain problems, ν is Poisson's ratio, and stress components in polar coordinates are shown in Equation (1). According to conditions shown in Equation (10), Ayatollahi, et al. [27] extracted the following equation for calculating the crack extension angle θ_m that corresponds to $S^{min}_{\theta\theta}$:

$$C_1K_I^2 + C_2K_{II}^2 + C_3K_IK_{II} + C_4(\beta\alpha K_{eff})K_I + C_5(\beta\alpha K_{eff})K_{II} + C_6(\beta\alpha K_{eff})^2 = 0.0 \tag{11}$$

C_1 to C_6 are shown in Appendix I. By calculating the crack extension angle θ_m from Equation (11) and substituting it in Equation (10), the general form of GS-criterion for crack growth under mixed mode loading can be obtained as follows:

$$\frac{8\pi G}{k-1}\left[A_1K_I^2 + A_2K_{II}^2 + A_3K_IK_{II} + A_4(\beta\alpha K_{eff})K_I + A_5(\beta\alpha K_{eff})K_{II} + A_6(\beta\alpha K_{eff})^2\right] - K_{IC}^2 = 0.0 \tag{12}$$

The fracture envelope under mixed mode loading can be predicted by the fracture resistance ratios K_I/K_{IC} and K_{II}/K_{IC} extracted from Equation (12) as follows:

$$\frac{K_I}{K_{IC}} = \left[\frac{8\pi G}{k-1}\left[A_1 + A_2M^2 + A_3M + A_4\left(\beta\alpha\sqrt{1+M^2}\right) + A_5\left(\beta\alpha M\sqrt{1+M^2}\right) + A_6\left(\beta\alpha\sqrt{1+M^2}\right)^2\right]\right]^{-\frac{1}{2}} \tag{13}$$

$$\frac{K_{II}}{K_{IC}} = \left[\frac{8\pi G}{k-1}\left[A_1M^{-2} + A_2 + A_3M^{-1} + A_4\left(\beta\alpha M^{-1}\sqrt{1+M^{-2}}\right) + A_5\left(\beta\alpha\sqrt{1+M^{-2}}\right) + A_6\left(\beta\alpha\sqrt{1+M^{-2}}\right)^2\right]\right]^{-\frac{1}{2}} \tag{14}$$

Mixed mode fracture stress $\sigma^f_{I/II}$ can be extracted from Equation (12) by substituting stress intensity factors K_I and K_{II} in this equation, and the dimensionless form of this stress can be shown as follows:

$$\sigma^f_{DIM} = \frac{1}{16\pi G}\frac{K^I_{dim}\sqrt{(k-1)(2+\beta\alpha) + \frac{k+1}{2}(\beta\alpha)^2}}{\sqrt{A_1{K^I_{dim}}^2 + A_2{K^{II}_{dim}}^2 + A_3K^I_{dim}K^{II}_{dim} + A_4\left(\beta\alpha K^I_{dim}\sqrt{{K^I_{dim}}^2 + {K^{II}_{dim}}^2}\right) + A_5\left(\beta\alpha K^{II}_{dim}\sqrt{{K^I_{dim}}^2 + {K^{II}_{dim}}^2}\right) + A_6\left(\beta\alpha\sqrt{{K^I_{dim}}^2 + {K^{II}_{dim}}^2}\right)^2}} \tag{15}$$

2.3. Generalized maximum tangential strain criterion (Gε-criterion)

This criterion states that a pre-existing crack in a brittle material can grow when the maximum tangential strain $\varepsilon^{max}_{\theta\theta}$ reaches the critical value of material strength ε_c at a critical radius r_c in front of the crack tip. The new crack orientation is perpendicular to that of $\varepsilon^{max}_{\theta\theta}$, and it forms an angle θ_m with the pre-existing crack's main plane. Equation (16) shows the tangential strain in its general form, while the angle θ_m can be found following conditions shown in in this equation [28,36,37]:

$$\varepsilon_{\theta\theta} = \frac{1+\nu}{E}[k\sigma_{\theta\theta} + (k-1)\sigma_{rr}] = \frac{1+\nu}{E\sqrt{2\pi r}}\left[D_1K_I + D_2K_{II} + D_3T\sqrt{2\pi r}\right], \tag{16}$$

$$\left.\frac{\partial \varepsilon_{\theta\theta}}{\partial \theta}\right|_{\theta=\theta_m} = 0.0, \left.\frac{\partial^2 \varepsilon_{\theta\theta}}{\partial \theta^2}\right|_{\theta=\theta_m} < 0.0$$

where D_1, D_2, and D_3 are shown in appendix I, E is Young's modulus, and $k = 1\text{-}\nu$ for plane strain problems. According to the conditions shown in Equation (16), the crack extension angle θ_m that corresponds to $\varepsilon^{max}_{\theta\theta}$ can be calculated using the following equation:

$$E_1K_I + E_2K_{II} + E_3\beta\alpha K_{eff} = 0.0 \tag{17}$$

E_1, E_2, and E_3 are shown in Appendix I. By calculating the crack extension angle θ_m from Equation (17) and substituting it in Equation (16), the general form of the Gε-criterion under mixed mode loading can be shown as follows:

$$\frac{D_1K_I + D_2K_{II} + D_3\beta\alpha K_{eff}}{(2k-1) + (k-1)\beta\alpha} - K_{IC} = 0.0 \tag{18}$$

The fracture resistance ratios K_I/K_{IC} and K_{II}/K_{IC}, which are taken from Equation (18), can be used to predict the fracture envelope under mixed mode loading using:

$$\frac{K_I}{K_{IC}} = \frac{(2k-1) + (k-1)\beta\alpha}{D_1 + D_2M + D_3\beta\alpha\sqrt{1+M^2}} \tag{19}$$

$$\frac{K_{II}}{K_{IC}} = \frac{(2k-1) + (k-1)\beta\alpha}{D_1M^{-1} + D_2 + D_3\beta\alpha\sqrt{1+M^{-2}}} \tag{20}$$

By substituting stress intensity factors K_I and K_{II} in Equation (18), the fracture stress $\sigma^f_{I/II}$ under mixed-mode loading can be calculated, and the dimensionless fracture stress under Gε-criterion can be expressed as:

$$\sigma^f_{DIM} = \frac{((2k-1) + (k-1)\beta\alpha)K^I_{dim}}{D_1K^I_{dim} + D_2K^{II}_{dim} + D_3\beta\alpha\sqrt{{K^I_{dim}}^2 + {K^{II}_{dim}}^2}} \tag{21}$$

It can be observed from the general governing equation of each fracture criterion that the GS and Gε criteria account for the effect of Poisson's ratio into account, whilst the Gσ-criterion is independent of it. This point may favor the GS and Gε criteria over the Gσ-criterion, especially in rock materials, where the Poisson's ratio has a significant impact on rock behaviour [38], brittleness index [39], and the transition from ductile to brittle behaviour [40]. Generalized fracture criteria consider the effect of critical distance from the crack tip (r_c) in contrast to the conventional fracture criteria [41]. The non-singular term in the stress distribution functions- the third term in equation (1) which includes the role of T-stress in the fracture process- was used to introduce the r_c parameter.

3. Materials and methods

In order to determine whether stress, energy, and/or strain-based fracture criteria may be used to predict fracture parameters at ambient, moderate, and elevated temperatures following thermal treatment. Two rock types were selected for this investigation. The mineralogical composition and grain size distribution of granite, the first type of rock, are shown in Fig. 1-a, and b, respectively. This rock type consists of 25 % quartz, 70 % plagioclase, and less than 5 % orthoclase and amphibole. Ninety percent of grains range in size from 278 µm to 1092 µm.

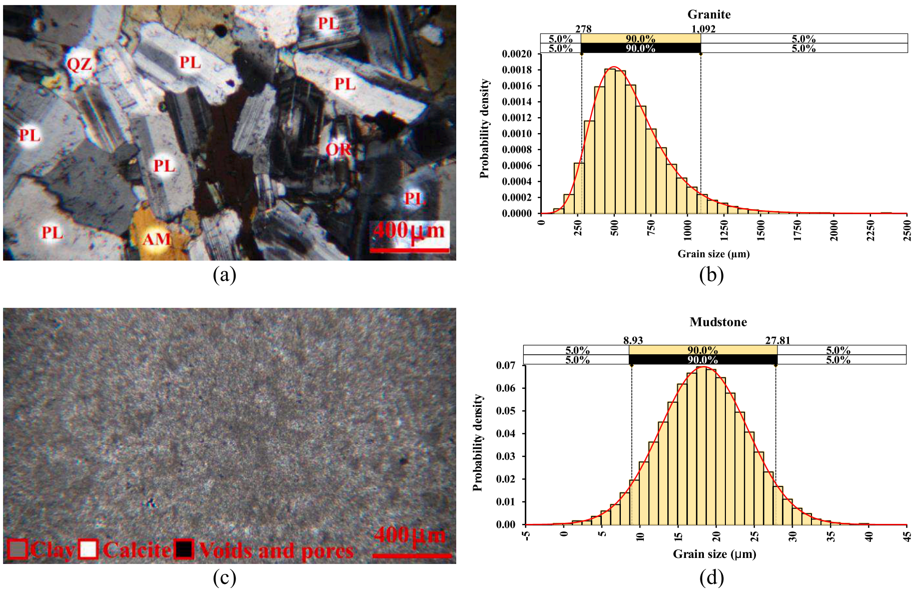

Fig. 1. (a, b) mineralogical composition and grain size distribution of granite, respectively, (c, d) mineralogical composition and grain size distribution of mudstone, respectively, (QZ: quartz, PL: plagioclase, OR, orthoclase, AM: amphibole).

Mudstone is the second type of rock selected for this investigation. Ninety percent of the grains in this mudstone are clay minerals with sizes of 8.93 μm to 27.81 μm, with the remaining eight percent being calcite, and two percent being pores and voids, as shown in Fig. 1-c,d.

The applicability of the generalized fracture criteria to predict fracture parameters of thermally treated rocks was investigated on those two rock types, which differ completely in mineral composition and their behavior in response to thermal effects [42–45].

3.1. Preparation of SCB specimens

Semi-circular specimens under the three-points bending test (SCB) are thought to be the most popular samples for studying the mechanical properties of fractures in rocks because they are easy to prepare from cylindrical cores. As a result, thirty-six SCB specimens from each rock type were prepared to undergo treatment at three different temperatures and tested under four different loading modes (pure mode I, 2 mixed mode loading I/II, and pure mode II). Prismatic samples were initially taken from the same rock block and examined visually for defects (Fig. 2-a,d). Next, 100 mm-diameter cylindrical cores were taken (Fig. 2-b,e). These cores were then sliced into disks with a thickness t of 35 mm. To create semi-circular specimens, each disk was then cut into two halves. Ultimately, a saw blade with a thickness of 1 mm was used to notch each SCB specimen, creating an edge notch with a length of $a = R/2 = 25$ mm (Fig. 2-c,f), where R is the radius of the SCB specimen. To obtain four distinct loading modes, a total of four notch inclination angles β were used; $\beta = 0.0^\circ$, to produce mode I, $\beta = 15$ and 30°, to obtain first and second mixed mode loading I/II with $K_{II}/K_I = 0.3$, and 0.75, respectively, and $\beta = 50^\circ$, to produce pure mode II (Fig. 2-f). For all loading modes, the distance between the two bottom supports is $2S = 60$ mm ($S/R = 0.6$). It should be noted that the geometry and dimensions of the SCB specimens were adopted based on the numerical simulation that was extensively illustrated in our previous works [44,45].

To ensure homogeneity across all SCB specimens for every rock type, the intactness criterion in the resulting granite and mudstone specimens was ensured based on the longitudinal wave velocity as an index to check the fissuring degree (IQ), $IQ\% = V_f/V_i \times 100$ [46]. Where V_f and V_i are the P-wave speeds of the fractured and intact rocks, respectively. The V_i of the intact granite and mudstone was measured and was found to be about 5500 and 4700 m/s. Then the V_f for all SCB specimens was measured and the fissuring degree IQ was calculated. It was found that the fissuring degree of all samples ranged between 96 % and 100 %, indicating non-fissured rock samples.

3.2. Thermal treatment

Rock samples were subjected to thermal treatment using the furnace seen in Fig. 3-a. This furnace may reach a maximum temperature of up to 1200 °C. The process of thermal treatment of the SCB specimens was done as follows: the temperature gradually increased linearly at a small rate of 4.2 °C/min until the desired temperature was reached. After reaching the set temperature, SCB specimens were kept for 24 h in the furnace under the desired temperature. After that, SCB specimens were naturally cooled to room temperature by opening the furnace door and leaving the samples to cool gradually until they returned to room temperature. The cooling rate was calculated based on the time required for the temperature of the rock samples to return to room temperature, and it was about 1 °C/min. Therefore, temperature gradient-induced thermal shock was avoided in the heating and cooling stage because the rock samples were gradually heated and cooled at a small rate of 4.2 °C/min and 1 °C/min, respectively [47–49]. Note that artificial notches were initially made in the SCB specimen before thermal treatment to increase the heat exposure surface, and to monitor the

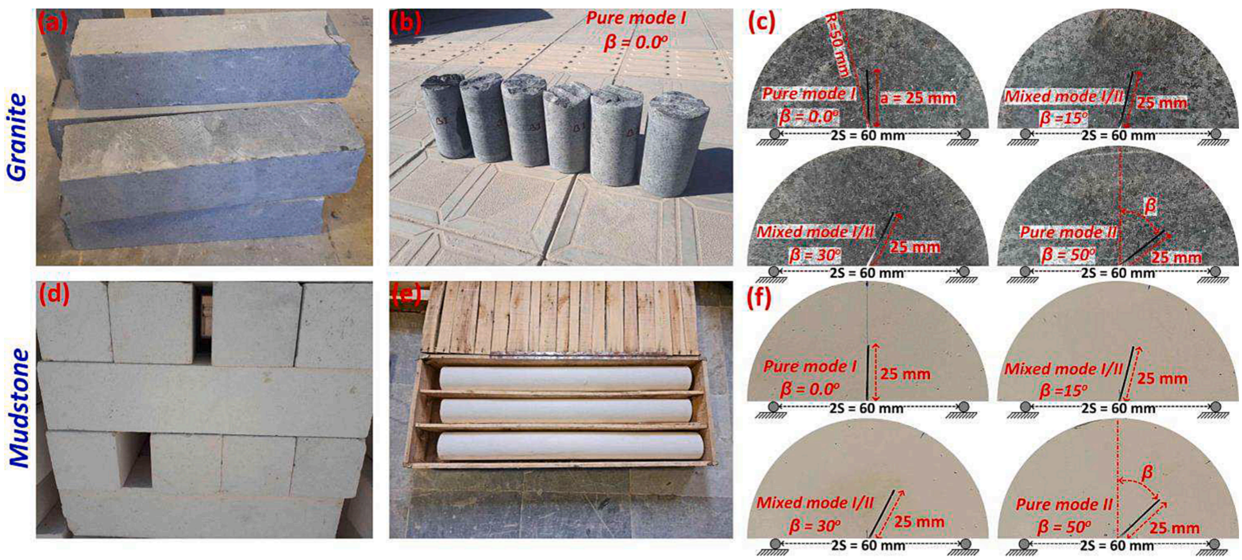

Fig. 2. Preparation of SCB specimens, (a to c) granite specimens, (d to f) mudstone specimens.

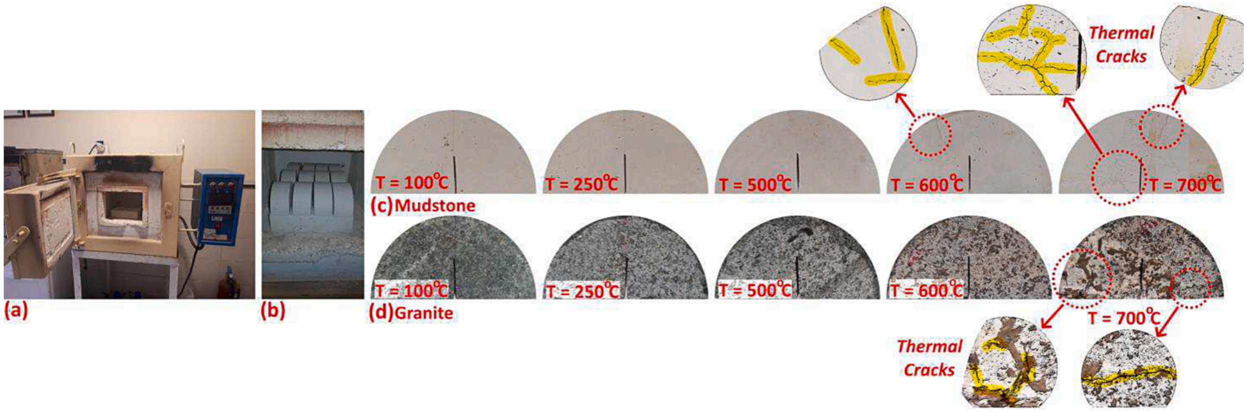

Fig. 3. Thermal treatment of SCB specimens, (a) the used furnace in the current study, (b) rock samples inside the furnace chamber, (c and d) SCB specimens of mudstone and granite after thermal treatment at a temperature between 100 and 700 °C, respectively.

possibility of thermal tensile fractures developing near the notch tip. In addition, this case is considered closer to reality because fracture surfaces in nature are directly exposed to the temperature, and therefore making a notch in SCB specimens allows for direct thermal impact on the fracture surface and its tip, which is considered the point of initiation and propagation of new cracks.

In order to determine the highest temperature that the investigated rock can withstand without the formation of thermal cracks, five rock samples of mudstone and granite were thermally treated in the furnace for 24 h at temperatures of 100, 250, 500, 600, and 700 °C. After that, the samples were closely visually inspected to see how the thermal cracks were developing on their surfaces. As shown in Fig. 3-c, no thermal cracks were detected on the mudstone samples after thermal treatment at temperatures of 100, 250, and 500 °C. Some thermal cracks, however, began to grow at 600 °C and a network of thermal fractures was observed after thermal treatment at 700 °C. Moreover, the granite utilized in this study withstood temperatures of up to 600 °C without developing surface thermal cracks, as shown in Fig. 3-d. Some thermal fractures were seen following the 700 °C thermal treatment. However, we found that the granite samples that were thermally treated at 600 °C became very weak and extremely brittle and were easily broken by mild taps with a small hammer.

It should be noted that the granite used in this study consists of 25 % quartz and this mineral undergoes α/β transition when the temperature exceeds 573 °C. The form of quartz under normal temperature is called α-quartz. By increasing the temperature above 573 °C, quartz undergoes a reversible change in crystal structure to form β-quartz [50]. This reversible change is called α/β transition of quartz and leads to the growth of thermal cracks. Griffiths, et al. [51] indicated that α/β quartz transition increases intergranular thermal stresses due to a large extension of material volume. In addition, studies in granite suggested that the aperture of thermal microcracks significantly increases when the temperature reaches the α/β quartz transition [52,53].

For mudstone, clay minerals that have a high affinity for water are the main constituent minerals in this rock type by 90 %. Water is removed during thermal treatment from clay minerals through two stages, dehydration and dihydroxylation [54]. The adsorbed, interlayer, and pore water is ejected in the dehydration process that can occur at T between 100 and 200 °C. In the second stage, the dihydroxylation process, hydroxyl ions leave the crystal structure of the clay minerals endorsing new thermal cracks to grow, propagate, and coalesce, as observed in Fig. 3-c after thermal treatment at 600 and 700 °C.

Based on the above, a maximum temperature of 500 °C was adopted to perform the experiments in this study. At this temperature,

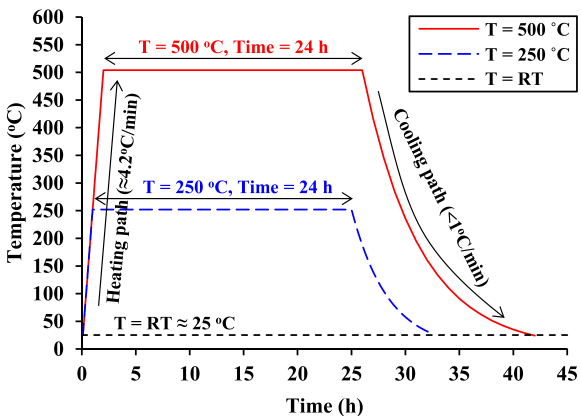

Fig. 4. Heating and cooling paths of the rock samples in the furnace.

no thermal fractures can grow due to α/β quartz transition in the granite, or due to the dihydroxylation process in the mudstone. Accordingly, SCB specimens for each rock type were split into three groups, each with twelve samples. The first group underwent testing at room temperature, while the second and third groups underwent thermal treatment at 250 and 500 °C in the furnace following the heating and cooling paths shown in Fig. 4 and then were tested at room temperature.

3.3. Three points bending test on SCB specimens

The three-point bending test was performed on the SCB specimens of granite and mudstone using the servo-hydraulic machine shown in Fig. 5. With a 20-ton capacity and vertical displacement speed range of 0.0001 to 250 mm/min, this machine is of type GOTECH AI-7000 LA 20. All SCB specimens were tested under a vertical speed of 1 mm/min in order to obtain a quasi-static strain rate (10^{-4} S^{-1}) that simulates rock mass behavior observed in mining, construction, excavation, etc. [55]. Four yellow copper tapes, as shown in Fig. 5, were glued to the specimens's faces to measure the fracture growth speed under different loading modes as discussed in our previous works [44,45].

4. Results and discussion

The primary outcomes of this study encompass the fracture behaviour, FPZ size, crack extension angle, fracture envelope, and dimensionless fracture stress that were predicted by both experimental and analytical methods. By predicting analytical results in SCB specimens and comparing them with experimental results, the effectiveness of the Gσ, GS, and Gε fracture criteria to predict fracture parameters in two types of thermally treated rocks with quite distinct mineralogical composition and mechanical behavior was investigated. Applying the generalized fracture criteria to SCB specimens, the following equations were used to calculate the specimens' K_I, K_{II}, and *T-stress*:

$$\begin{aligned} K_i &= \frac{P}{2Rt} K^i_{dim}\sqrt{\pi a}, (i = I, II) \\ T &= \frac{P}{2Rt} T_{dim} \end{aligned} \tag{22}$$

where P is the load applied on the SCB specimen. At the onset of fracture, $P = P_{cr}$, and the fracture toughness K_{ic} (i = I, II) can be obtained. In Alneasan and Alzo'ubi's [44,45] work the dimensionless stress intensity factors K^i_{dim} (i = I, II) and *T-stress* (T_{dim}) for SCB specimens with the geometry presented in section 3.1 were numerically derived as a function of the notch inclination angle as follows:

$$\begin{aligned} K^I_{dim} &= 4.195 - 1.229 \bullet 10^{-2}\beta - 3.227 \bullet 10^{-3}\beta^2 + 3.606 \bullet 10^{-5}\beta^3 \\ K^{II}_{dim} &= -6.61 \bullet 10^{-3} + 9.837 \bullet 10^{-2}\beta - 2.002 \bullet 10^{-3}\beta^2 + 8.536 \bullet 10^{-6}\beta^3 \\ T_{dim} &= -5.443 \bullet 10^{-1} + 5.485 \bullet 10^{-2}\beta + 2.907 \bullet 10^{-3}\beta^2 - 4.619 \bullet 10^{-5}\beta^3 \\ & \beta indegrees \end{aligned} \tag{23}$$

4.1. The effect of temperature and loading mode on the fracture behaviour

Many studies on rocks have revealed that the behaviour of rock fractures can change with temperature, and when the temperature rises above a particular threshold, brittle-ductile transformation can occur. According to Wang, et al. [42], granite undergoes a brittle-ductile transformation as a result of temperature changes, which alters the rock fracture toughness. Yin, et al. [56] showed that the start temperature for the brittle-ductile transformation of thermally treated SCB specimens of Fujian granite is 300 °C. Nasseri, et al. [52] demonstrated that the sudden drop in fracture toughness of Westerly granite, referred to as the brittle-ductile transition, is at

Fig. 5. Servo hydraulic machine used in this study with set up of three points bending test to obtain four different mode mixites in mudstone and granite samples.

temperatures between 450 °C and 650 °C. To show the effect of temperature and loading mode on the fracture behaviour in granite and mudstone, load–displacement curves of some SCB specimens of granite and mudstone are shown in Fig. 6.

For the granite samples under pure mode I, $\beta = 0°$, (Fig. 6-a), the fracture grows brittlely at T = RT (G-0-RT) and 250 °C (G-

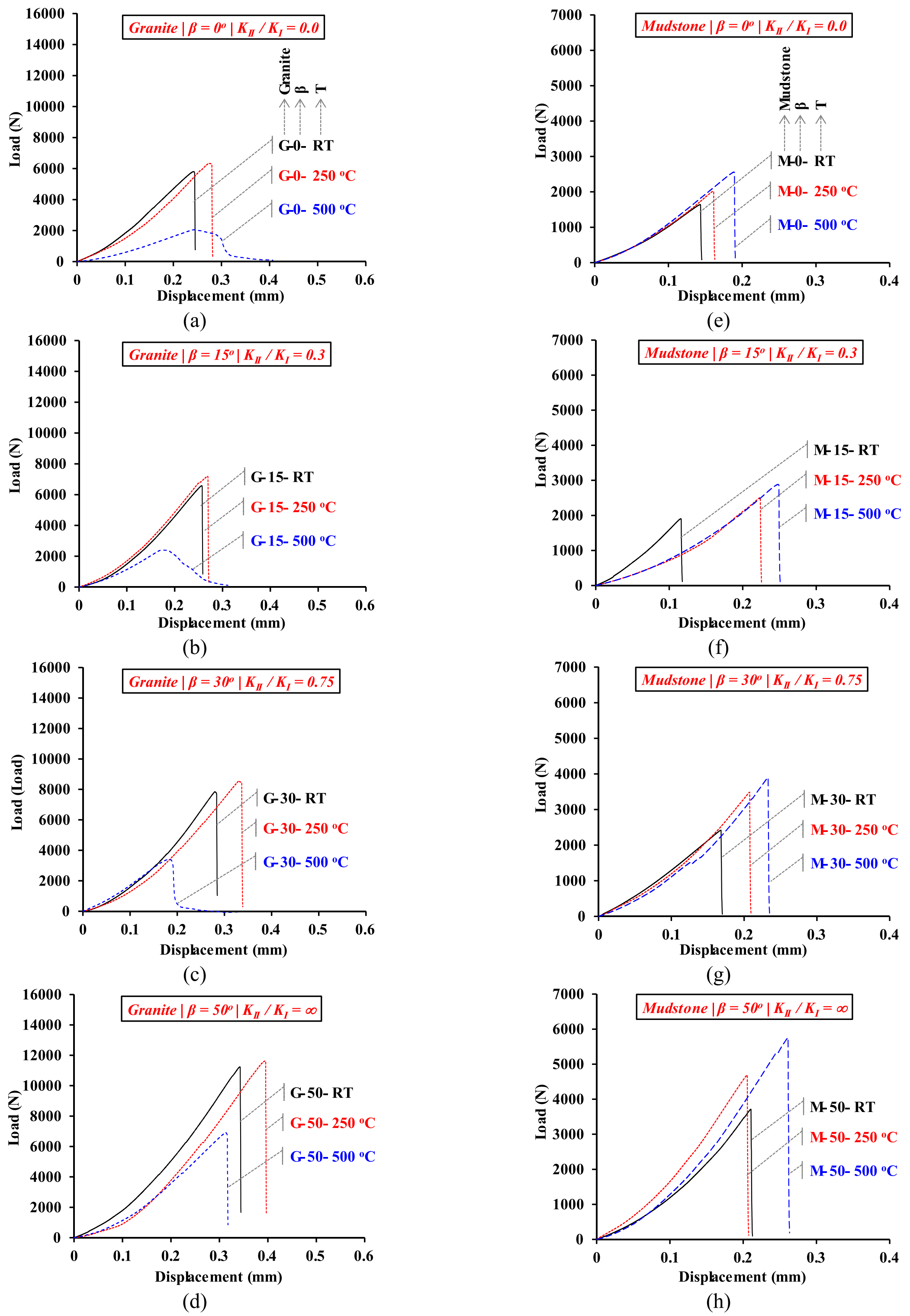

Fig. 6. Displacement-Load curves for some SCB specimens of (a, b, c and d) granite and (e, f, g, and h) mudstone.

0–250 °C) and ductility at T = 500 °C (G-0–500 °C). At T = RT and 250 °C, the load–displacement curve drops abruptly at the moment of fracture (brittle behaviour). However, post-peak plastic behaviour is evident at T = 500 °C (ductile), the same points can be observed for the granite under mixed mode loading I/II for $\beta = 15^\circ$ ($K_{II}/K_I = 0.3$, Fig. 6-b). At all temperatures, no ductile behavior for fracture is found for $\beta = 30^\circ$ ($K_{II}/K_I = 0.75$, Fig. 6-c) and $\beta = 50^\circ$ (pure mode II, Fig. 6-d). Thus, it can be concluded that depending on the temperature and loading mode, the fracture in the granite can grow in a brittle or ductile manner. A transition from brittle to ductile behaviour can occur at temperatures between 250 and 500 °C when the mode mixity ratio is low. As this ratio rises, the fracture growth approaches pure mode II and exhibits a more brittle fracture behaviour.

It can be observed that in the case of the mudstone samples, the fracture only grows brittlely under all temperature and loading mode conditions. Fracture load is directly proportional to the temperature and mode mixity ratio in the mudstone samples. In granite, the fracture load rises as the temperature rises from RT to 250 °C, after which it decreases as the temperature rises to 500 °C. Therefore, it can be said that increasing the temperature of thermal treatment in the mudstone increases its brittleness and reduces its ductility. While in granite, increasing the temperature to a certain limiting value, T_l, between 250 °C and 500 °C increases its brittleness at the expense of its ductility (further investigations are needed to determine the exact value of T_l). Contrarily, for temperatures greater than T_l, increasing the temperature leads to an increase in the fracture ductility at the expense of its brittleness. In addition, increasing the mode mixity ratio enhances the brittleness of the fracture. The brittleness degree changes in granite and mudstone are explained later in Section 4.3 based on Poisson's ratio.

4.2. Calibration of FPZ based on generalized fracture criteria

The generalized fracture criteria are functions of two significant physical parameters, Poisson's ratio (ν) and the critical distance from the crack tip, r_c, which in rock mechanics denotes the radius of the FPZ. This was demonstrated earlier in the analytical phase of this study. Table. 1 provides a summary of Poisson's ratio as a function of temperature for the mudstone and granite used in this work. The r_c is generally considered a material property that is independent of specimen geometry and loading conditions [57,58]. This property can be estimated based on the ratio of mode I fracture toughness, K_{IC}, and material tensile strength (σ_t) using the following equation [59].

$$r_c = \frac{1}{2\pi}\left(\frac{K_{IC}}{\sigma_t}\right)^2 \tag{24}$$

According to Meng, et al. [12], as K_{IC} and σ_t are inherent properties of the material, the K_{IC}/σ_t ratio ought to be constant and independent of other factors like temperature. Accordingly, Equation (24) yields a constant value for r_c at any temperature. This seems counterintuitive as other scholars have emphasized that the FPZ size should not be constant [23,60,61]. Additionally, since Equation (24) is essentially a function of experimentally measurable parameters in pure mode I, this equation may give a reasonable value for FPZ only under that mode. Wei, et al. [62] calibrated r_c based on Equation (24) and the equations of the maximum normal strain criterion (MNSN), and found that the second method is more suitable to determine r_c because it considers the non-singular strain terms. As a result, the FPZ size was estimated in this study using three different fracture criteria as well as by accounting for pure mode I and II fracture toughness; two important parameters in rock fracture mechanics. To estimate r_c in this study, pure mode I and II fracture toughness were experimentally measured and the ratio K_{IIC}/K_{IC} was plotted independently of r_c in Fig. 7, shown as a black continuous line in this figure. Then the analytical K_{IIC}/K_{IC} was predicted using the three generalized fracture criteria and plotted in Fig. 7 as a function of r_c. The r_c was adopted based on the intersection between the analytical and experimental fracture toughness ratio (Fig. 7). For instance, at room temperature, experimental results gave an average value of K_{IIC}/K_{IC} measured using three SCB specimens of granite of 0.477. Fig. 7-a shows that Gσ, GS, and Gε can predict the experimental K_{IIC}/K_{IC} at $r_c = 0.85$, 1.67, and 0.12 mm, respectively. Similarly, the r_c was predicted using the generalized fracture criteria in the granite and mudstone at room temperature, moderate (250 °C), and elevated (500 °C) temperature conditions. Fig. 7-c also demonstrates that the Gε criterion cannot predict the K_{IIC}/K_{IC} at T = 500 °C for any value of the r_c. Furthermore, Fig. 7-d, e, and f demonstrate that the Gε-criterion was unable to predict the K_{IIC}/K_{IC} at all temperature conditions for any value of the r_c. Therefore, the strain-based criterion in this study (Gε-criterion) is no longer

Table 1
Poisson's ratio and tensile strength of the granite and mudstone at three temperatures of RT, 250 and 500 °C, and the critical distance from the crack tip extracted from Fig. 7.

Temperature (°C)	Property	Granite			Mudstone		
		Gσ	GS	Gε	Gσ	GS	Gε
RT	ν	0.23			0.377		
	r_c (mm)	0.85	1.67	0.12	0.41	0.3	–
	σ_t (MPa)	10.3			3.2		
250	ν	0.2			0.335		
	r_c (mm)	0.9	1.93	0.22	0.4	0.49	–
	σ_t (MPa)	12.3			4.5		
500	ν	0.27			0.303		
	r_c (mm)	0.055	0.2	–	0.37	0.59	–
	σ_t (MPa)	4.9			6.1		

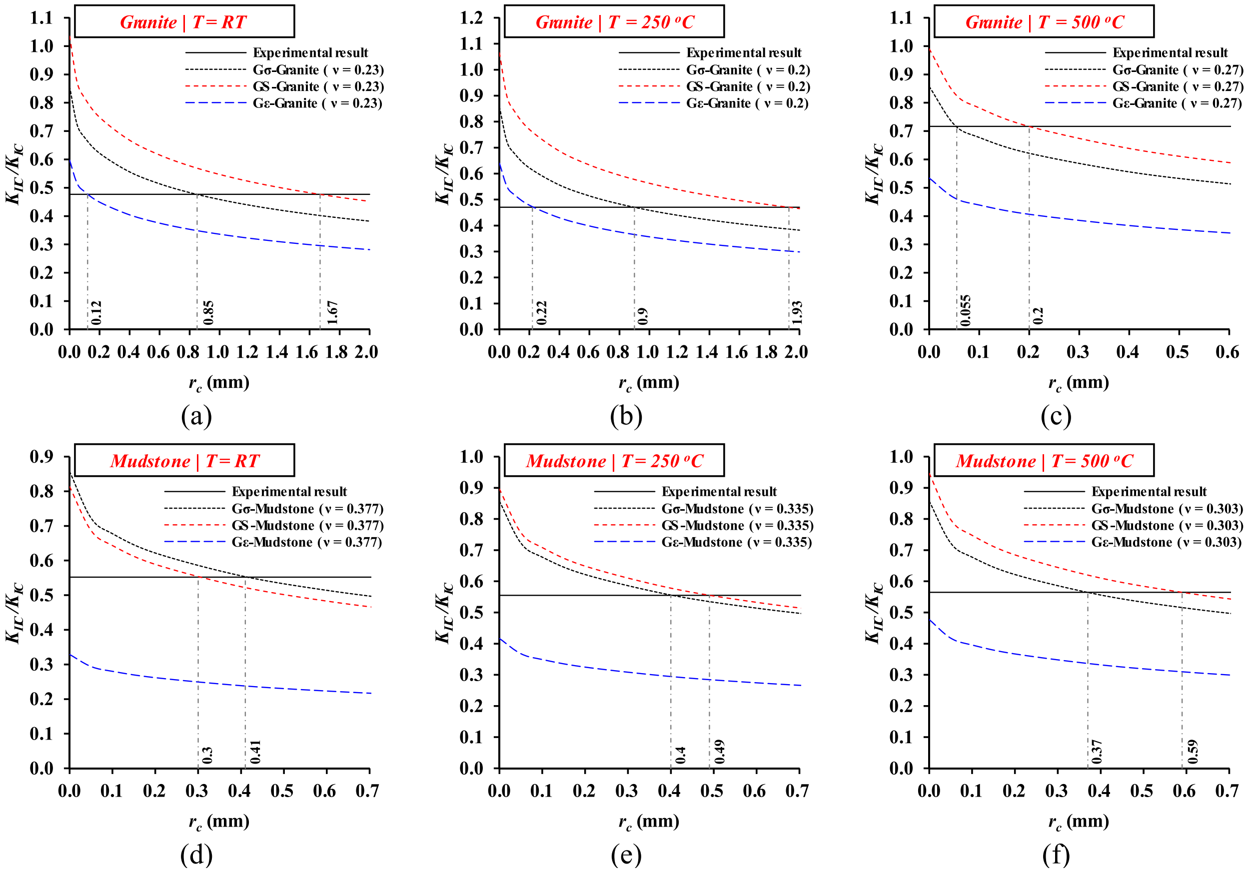

Fig. 7. Prediction of the critical distance from the crack tip in the granite under (a) RT, (b) 250 °C, and (c) 500 °C and in the mudstone under (d) RT, (e) 250 °C and (c) 500 °C using Gɕ, GS and Gε fracture criteria.

applicable for granite that has undergone thermal treatment at 500 °C and for mudstone at any temperature.

4.3. Thermal treatment effect on the FPZ size

The fracture process zone size (r_c) is an essential parameter affecting the accuracy of generalized fracture criteria in predicting fracture characteristics. This parameter cannot be treated as an inherent property of the material, independent of the influence of external factors such as temperature. The effect of temperature on this parameter in granite was extensively investigated by some researchers in the literature [22,32,63]. Feng, et al. [32] concluded that the theoretical estimations of the Gσ criterion differ significantly from the experimental results because the FPZ size calculated by the conventional method (equation (24)) was larger than that derived from experimental data, and they introduced a correction factor for the FPZ size as a function of temperature. In addition, Feng, et al. [32] estimated the FPZ radius using Equation (24) for different rock types tested by other researchers [64–68] and concluded that the FPZ size decreases with temperature increase. Regarding the effect of temperature on the FPZ size of granite and mudstone tested in our study, Table. 1 summarizes the predicted values of r_c using the three generalized fracture criteria in granite and mudstone at different temperature conditions. Note that the energy-based criterion predicts a greater FPZ size in granite than the stress and strain-based criteria. The three generalized fracture criteria in the granite showed that the r_c increases for T between RT and 250 °C and subsequently decreases for T between 250 °C and 500 °C, with the brittleness of the fracture having the largest effect. Gɕ-criterion predicts r_c larger than that predicted by the GS-criterion for the mudstone under room temperature. However, the r_c predicted by the GS-criterion is greater than that predicted by the Gɕ-criterion for T = 250 °C and 500 °C. When the temperature increases from RT to 500 °C, the FPZ size predicted by the Gɕ criterion drops from 0.41 to 0.37 mm indicating that it is not extremely sensitive to temperature. Even though the energy-based criterion shows that the FPZ size noticeably increases when the temperature increases from RT to 500 °C.

Based on the above, the FPZ radius is greatly affected by temperature and is directly proportional to the rock behaviour. By increasing temperature from RT to 250 °C, Fig. 6-a to d indicated an increase in the fracture load of granite, and the three generalized fracture criteria in Table. 1 indicated an increase in the FPZ size. While for T between 250 °C and 500 °C, the fracture load decreased, and the three generalized fracture criteria indicated a sharp decrease in the FPZ size. For the mudstone, Fig. 6-e to h showed a direct proportional between temperature and fracture load, and the GS criterion in Table. 1 showed the same trend between temperature and

FPZ size. When the rock properties improve with temperature increase, the microstructure of the rock at the notch tip becomes less broken, and the new crack needs a longer distance from the notch tip to reach the critical strength of the material, and the opposite is true when the rock properties deteriorate with temperature increase.

4.4. *The effect of thermal treatment and loading mode on brittleness index*

To quantitively show the effect of temperature on brittleness index (*BI*) and FPZ size (r_c), the brittleness index under three points bending test was calculated based on the equation provided by Tarokh, et al. [69] which takes the effect of tensile strength (σ_t) and pure mode I fracture toughness (K_{IC}) into account, equation (25). *D* in this equation is the structure size parameter, such as diameter in SCB specimens. Because all SCB specimens in this study have the same dimensions, *BI* can be normalized to *D* as *BI/D*. Our tests were conducted under four mode mixities, to take the effect of loading mode into account, K_{IC} in equation (25) was replaced by K_{EC}, where K_{EC} is the effective fracture toughness, in equation (26). For tensile strength, this parameter was measured in this study based on the Brazilian tensile strength test and the results are shown in Table. 1. It can be noted that the tensile strength in the mudstone is directly proportional to the temperature, while in the granite, the tensile strength first increases and subsequently decreases as the temperature exceeds 250 °C. The Brittleness index is shown in Fig. 8 as a function of notch inclination angle (mode mixity ratio) and temperature. Fig. 8-a shows that the *BI* is directly proportional to the temperature. By increasing β from 0 to 15°, the *BI* slightly decreases and then it sharply increases after β of 15°. Fig. 8-a demonstrates that the *BI* and the r_c estimated by the GS-criterion increase with increasing temperature. Fig. 8-b shows that the *BI* has the same trend of other mechanical parameters in granite under the effect of temperature, it increases in the temperature range between RT and 250 °C, and then it significantly decreases after thermal treatment at 500 °C. In addition, it can be noted that the *BI* slightly decreases with increasing β to 15°, and then it sharply increases after β of 15°. Fig. 8-b shows that the *BI* and r_c estimated by Gσ and GS criteria are directly and inversely proportional to the temperature in the ranges of RT to 250 °C, and 250 to 500 °C, respectively. In addition, Fig. 8 demonstrates that the brittleness index in the mudstone and granite significantly increases with approaching mode II conditions, $\beta = 50°$, indicating that mode II fractures are more brittle than mode I fractures.

$$BI = D\left(\frac{\sigma_t}{K_{IC}}\right)^2 \tag{25}$$

$$\frac{BI}{D} = \left(\frac{\sigma_t}{K_{EC}}\right)^2, K_{EC} = \sqrt{K_{IC}^2 + K_{IIC}^2} \tag{26}$$

Tarokh, et al. [69] did not provide a limit of *BI* for the transition from brittle to ductile behaviour. Therefore, this limit was approximately estimated in this study based on the displacement-load curves of granite. G-0–500, G-15–500, and G-30–500 in Fig. 6 show post-peak ductile behaviour, while G-50–500 shows brittle post-peak behavior. Therefore, the transition from brittle to ductile behaviour can be approximately determined between G-50–500 and G-30–500. The average *BI* of G-30–500 and G-50–500 is about 40. The average *BI* in the granite was calculated for each temperature, and the results are plotted in Fig. 9, this figure shows that the transition from brittle to ductile behaviour in the granite can approximately occur at a temperature of 460 °C. For the mudstone, the transition from semi-ductile to brittle behaviour was not determined because the displacement-load curves of the mudstone shown in Fig. 6 did not show any post-peak ductile behavior. But based on Fig. 8-a, it can be said that the brittleness degree of the mudstone increases as temperature increases.

4.5. *Fracture envelope*

In rock mechanics, fracture envelopes are important to determine the circumstances that a crack undergoes when growing under

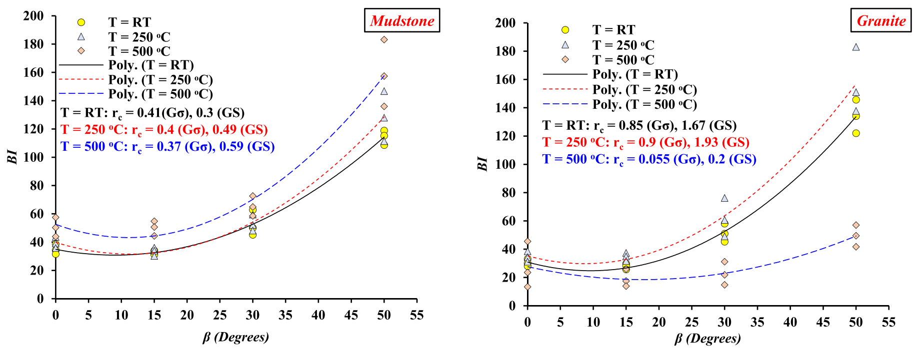

(a) (b)

Fig. 8. Brittleness index in (a) mudstone and (b) granite as a function of notch inclination angle and temperature.

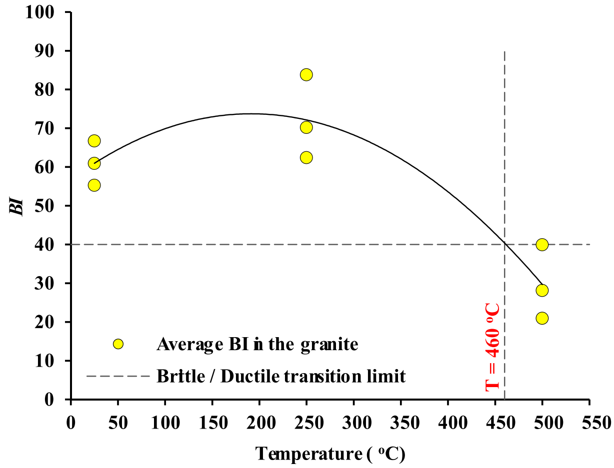

Fig. 9. Approximation method to determine brittle/ductile transition limit in the granite.

mixed mode loading. In this study, fracture envelopes were predicted using the generalized fracture criteria in thermally treated SCB specimens of granite and mudstone. The results are presented in Fig. 10. In general, it can be observed that the Gσ and GS fracture criteria can provide a good estimation of the fracture envelope both before and after thermal treatment when compared to the experimental results. However, compared to the Gσ-criterion, the GS-criterion can yield an analytical fracture envelope that more closely matches the experimental results. This can be attributed to the fact that the energy-based criterion (GS-criterion) considers the effect of two important rock physical parameters: Poisson's ratio and the critical distance from the crack tip. In contrast, the stress-

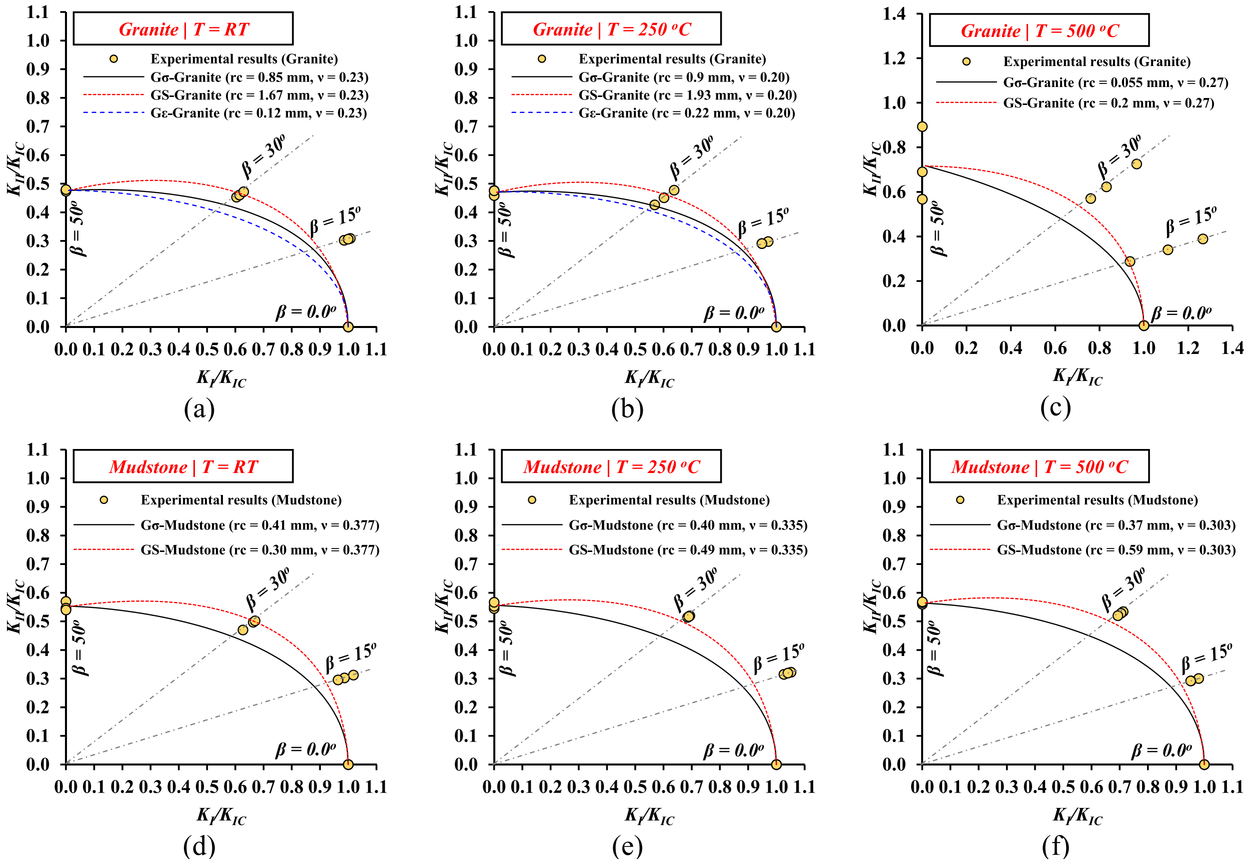

Fig. 10. (a, b and c) Fracture envelopes predicted in the granite at T = RT, 250 and 500 °C, respectively, (d, e, and f) fracture envelopes predicted in the mudstone at T = RT, 250 and 500 °C, respectively.

based criterion (Gσ-criterion) considers the effect of just one physical parameter into account, which is the r_c. The Poisson's ratio in the GS criterion is considered a crucial parameter in describing the changes in the brittleness degree of the rock with thermal treatment.

Two trends of behaviours were observed in granite; in the first regime, ν decreased from 0.23 at T = RT to 0.2 at T = 250 °C, indicating an increase in the brittleness degree of the rock after thermal treatment at 250 °C. This decrement in Poisson's ratio was due to the development of some isolated thermal micro-fractures in the rock samples. These fractures obstruct the growth of the main fracture under the effect of external loads due to their direction is not in the favorable direction of the main fracture [70]. On the other hand, in the second regime, ν increased from 0.23 at T = 250 °C to 0.27 at T = 500 °C, indicating a decrease in the brittleness degree of this rock type after thermal treatment at 500 °C. This decrease in the brittleness of the granite is due to the coalescence of thermal micro-fractures that form continuous surfaces of weakness in the rock sample [71,72]. The changes occurring in the SCB granite specimens during thermal treatment were considered in the GS-criterion through Poisson's ratio. Therefore, the results of this criterion were more consistent with the experimental results than those of the Gσ-criterion.

For mudstone, however, only one regime was observed in this rock type, with improvement in the mechanical properties as temperature increased from RT to 500 °C. This improvement was due to the drying of clay minerals that form 90 % of this rock type during the dehydration and dehydroxylation processes. The mudstone became more brittle as it dried progressively, and a gradual transition from semi-ductile to completely brittle behavior occurred. Consequently, the Poisson's ratio decreased from 0.377 at T = RT to 0.335 at T = 250 °C and 0.303 at T = 500 °C [73]. As a result of accounting for Poisson's ratio, in the GS-criterion, the fracture envelopes predicted by this criterion have good agreement with the experimental results. On the other hand, the Gσ-criterion predicts lower envelopes than the experimental results as demonstrated in Fig. 10-d, e, and f.

4.6. Fracture stress

The second parameter that can be predicted using the fracture criteria is the fracture stress, which is an important parameter, both in the laboratory and in situ. This parameter can be predicted in non-dimensional form ($\sigma^f_{I/II}/\sigma^f_I$) as the fracture toughness ratio (K_{IIC}/K_{IC}), using Equations (9), 15, and 21 for the Gσ, GS, and Gε criteria, respectively. When the mode I fracture stress σ^f_I is known, dimensionless fracture stress predicted using the fracture criteria is important to determine the maximum load needed to break the rock samples in the laboratory under different loading modes, i.e., at any mode mixity ratio K_{II}/K_I. This will help us determine the

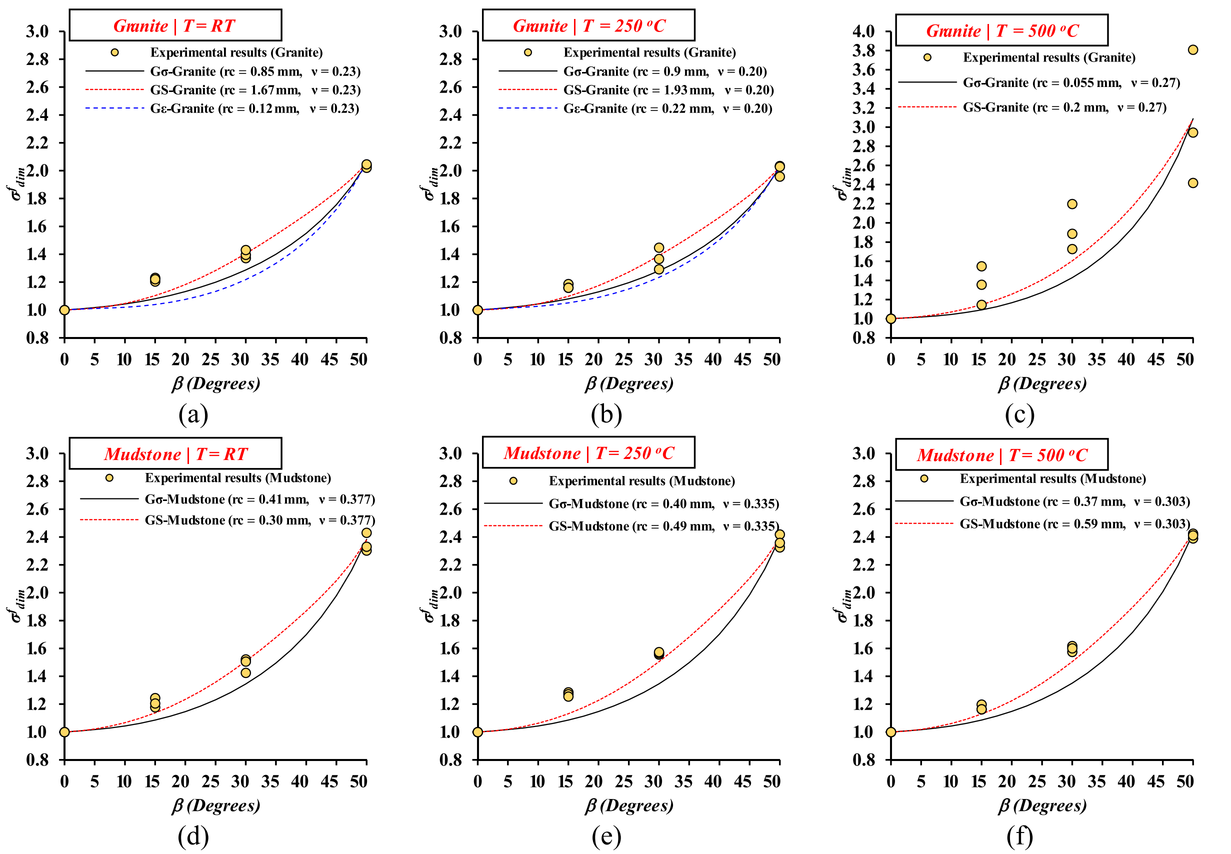

Fig. 11. (a, b and c) dimensionless fracture stress predicted in the granite at T = RT, 250 and 500 °C, respectively, (d, e and f) dimensionless fracture stress predicted in the mudstone at T = RT, 250 and 500 °C, respectively.

capacity of the loading device used to test rock samples under different loading modes. For a crack in a rock mass, fracture stress is important to determine if this crack can grow under the influence of in situ stresses. Dimensionless fracture stress predicted in the SCB specimens of granite and mudstone using the generalized fracture criteria are shown in Fig. 11. It can be noted that the GS-criterion can estimate a more accurate value for this stress, although the Gσ-criterion predicts σ^f_{dim} in granite and mudstone less accurately than experimental results.

4.7. Crack extension angle

Crack extension angle is an important parameter in rock fracture mechanics to predict the preferred direction of a new fracture under different loading modes and the influence of various environmental factors, such as temperature, which is investigated in this study. Therefore, the results of the crack extension angle were presented and discussed from two angles. The first viewpoint includes the effect of temperature on this angle and the fracture path as a whole. The second point of view includes the ability of the generalized fracture criteria to predict this angle.

4.7.1. Crack extension angle versus temperature effect

The crack extension angle can be experimentally measured as the angle between the plane of the notch and the initial step of the

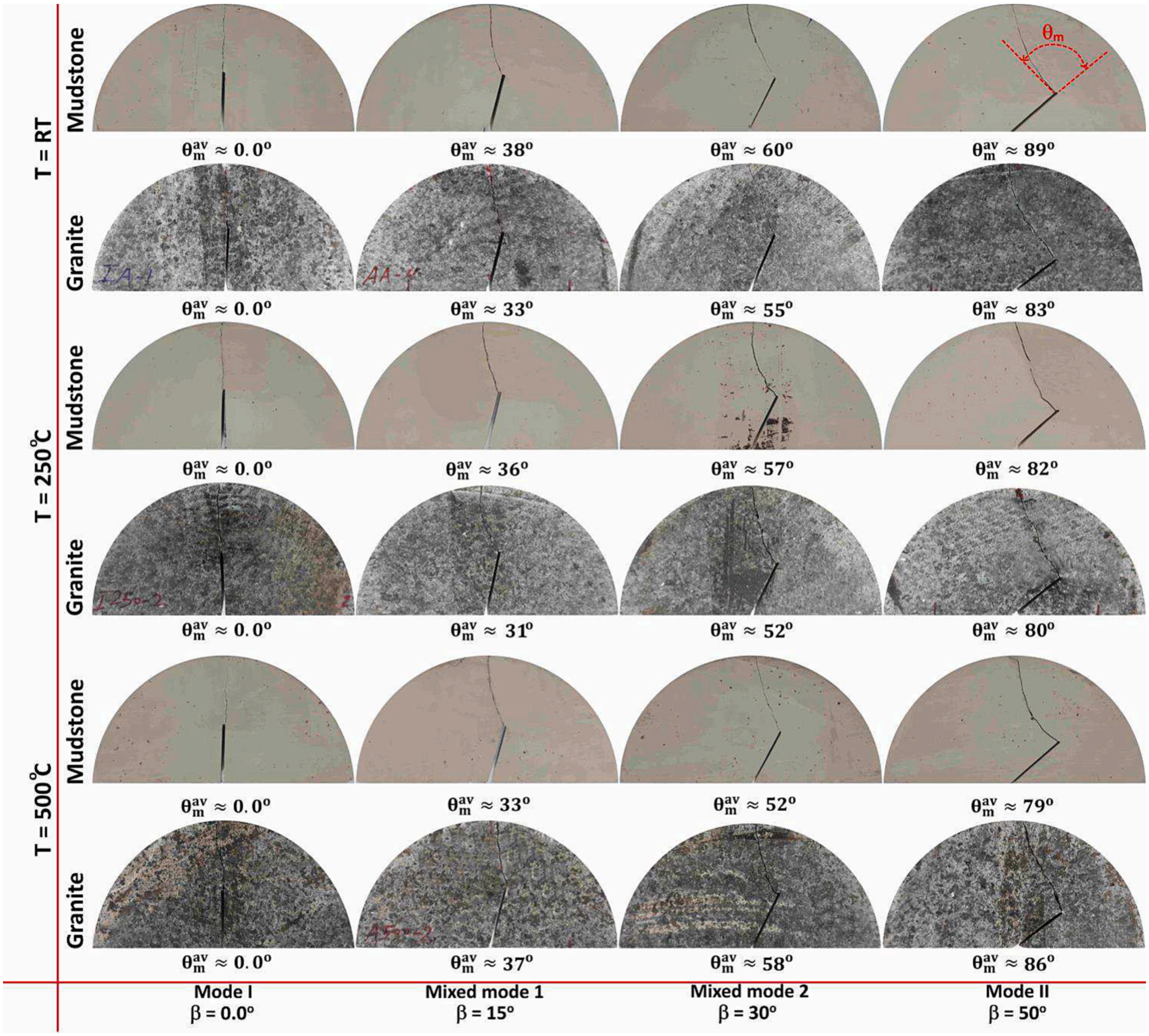

Fig. 12. Crack extension angle and fracture trajectories predicted experimentally in SCB specimens of granite and mudstone at T = RT, 250 and 500 °C.

new fracture. Crack extension angle and fracture trajectories predicted experimentally in the SCB specimens of granite and mudstone at T = RT and after thermal treatment at T = 250 and 500 °C are displayed in Fig. 12. Under pure mode I ($\beta = 0.0°$), the fracture grows in an essentially straight line between notch tip and the point of applying external load (specimen top). By increasing the notch inclination angle, or in other words increasing mode mixity ratio $M = K_{II}/K_I$, the fracture trajectory's curvature increases. In general, the fracture path follows an almost straight or curved path from the notch tip to the location where an external load is applied. No specific effect of rock type or thermal treatment on the overall fracture path was observed. The crack extension angle was the only place where the rock type and thermal treatment had an impact. Fig. 12 shows that for mudstone, which has a single regime against temperature effect, the crack extension angle decreases with increasing temperature from RT to 250 and 500 °C. In granite, which behaves in two regimes once subjected to thermal treatment, the crack extension angle decreases with increasing temperature from RT to 250 °C, and then it increases as temperature rises to 500 °C.

The average values of θ_m, K_{IC}, and K_{IIC} measured experimentally in the laboratory are shown in Fig. 13 as a function of temperature and notch inclination angle. This figure concludes that the crack extension angle measured in granite and mudstone are inversely proportional to the mechanical properties, which include mode I and II fracture toughness. By increasing T from RT to 250 °C in granite, K_{IC} and K_{IIC} increase, and θ_m decreases, and vice versa for T between 250 and 500 °C. In mudstone, however, increasing T from RT to 250 °C and then to 500 °C caused K_{IC} and K_{IIC} to increase and θ_m to decrease. The reasons behind the observed behavior in mudstone and granite after thermal treatment were briefly explained in section 4.3 and extensively discussed in Alneasan, et al. [74].

4.7.2. *Prediction of the crack extension angle using generalized fracture criteria*

The crack extension angle was analytically predicted using generalized fracture criteria before and after thermal treatment by considering ν and r_c, and the results are summarized in Table. 1. Fig. 14 shows the analytical and experimental results of the crack extension angle. This figure shows that for T = RT (Fig. 14-a) and T = 250 °C (Fig. 14-b) in granite, the analytical results predicted using the GS criterion are in good agreement with the corresponding experimental data. The energy-based criterion achieves higher agreement with the experimental results, although the stress and strain-based criteria can predict the crack extension angle effectively. Following the thermal treatment of granite at 500 °C, the Gσ and GS fracture criteria predict a crack extension angle somewhat smaller than the experimental value, see Fig. 14-c.

For mudstone under natural conditions (T = RT, Fig. 14-d), the Gσ and GS fracture criteria predict a crack extension angle slightly less than the experimental data. The GS-criterion gives a good estimate for θ_m under pure mode II ($\beta = 50°$). After thermal treatment at 250 °C (Fig. 14-e), the analytical results predicted by the stress and energy-based criteria become more in line with the experimental results. The best agreement between the analytical and experimental results is found at T = 500 °C.

5. Limitations and future directions

The effect of thermal treatment on the fracture behaviour of granite and mudstone in this study was limited to a temperature range that does not include the development of thermal fractures. The maximum temperature was 500 °C, this temperature is less than α/β quartz transition in granite and lower than the dihydroxylation process limit in the mudstone. For future works, we recommend investigating fracture behaviour in the granite and mudstone at a temperature greater than 500 °C, and checking the applicability of stress, strain, and energy-based criteria to predict fracture parameters above this temperature. In addition, we recommend using some experimental techniques such as scanning electron microscope (SEM) to deeply investigate the effect of temperature on the fracture process zone and to analyze the fracture surfaces to further examine the characteristics of brittle fractures, plastic deformations, and other traces at different temperatures.

6. Conclusions

This study examined the behaviour of rock fracture in granite and mudstone in response to thermal effects to evaluate the power of the stress, energy, and strain-based criteria in predicting fracture parameters both before and after thermal treatment. 72 SCB specimens of the rock types were prepared and tested at normal (T = RT), moderate (T = 250 °C), and elevated (T = 500 °C) temperature conditions under four mode mixites (pure mode I, 2 mixed mode loading I/II, and pure mode II). The following describes the study's overall conclusions:

- Raising the mudstone's thermal treatment temperature from room temperature to 250 °C and then to 500 °C increases brittleness and decreases ductility. In granite, increasing temperature to a certain limit between 250 °C and 500 °C enhances brittleness at the expense of ductility. If temperatures are risen higher than this point, the opposite occurs. Moreover, a higher mode mixity ratio makes the fracture more brittle.
- The FPZ size is proportional to the brittleness degree of the two rock types tested in this study, and the thermal treatment temperature has a significant impact on this relationship. Except for T = 500 °C, the size of FPZ as measured by r_c in granite is greater than that in mudstone. In addition, the FPZ size predicted by the energy-based criterion is larger than the one predicted by the stress and strain-based criteria.
- The strain-based criterion was no longer useful for predicting the fracture parameters in granite after thermal treatment at T = 500 °C and in mudstone at any temperature. The energy-based criterion is superior to the stress-based criterion for predicting the fracture parameters before and after thermal treatment because it takes the effect of Poisson's ratio into account, which reflects the changes in the brittleness degree of the material well when temperature changes.

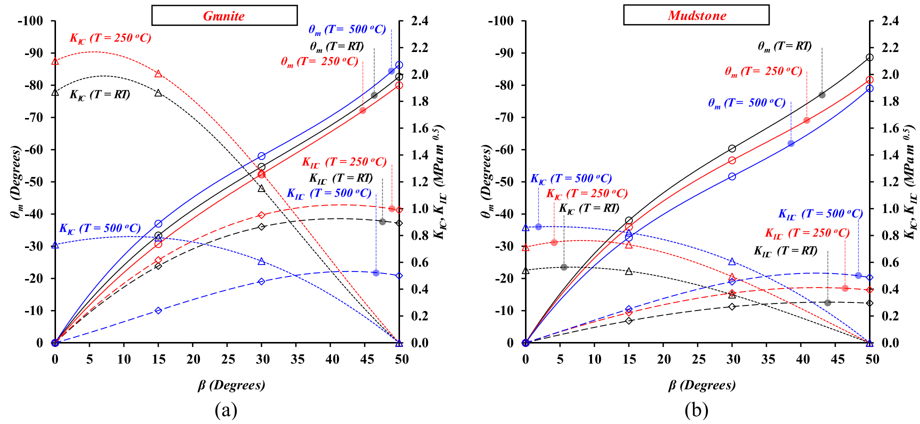

Fig. 13. The average values of θ_m, K_{IC}, and K_{IIC} measured experimentally in the laboratory as a function of temperature and notch inclination angle.

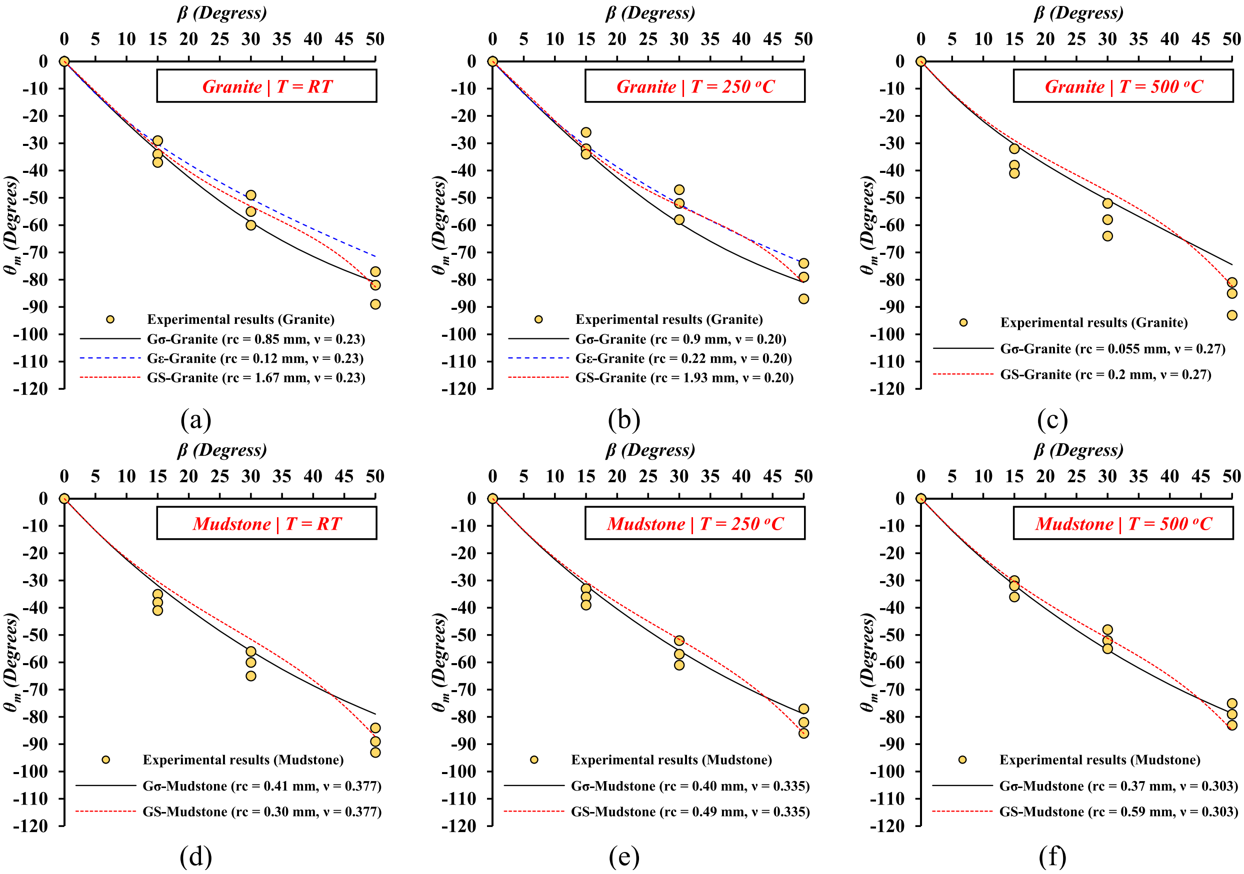

Fig. 14. (a, b and c) crack extension angle predicted in the granite at T = RT, 250 and 500 °C, respectively, (d, e, and f) crack extension angle predicted in the mudstone at T = RT, 250 and 500 °C, respectively.

CRediT authorship contribution statement

Abdel Kareem Alzo'ubi: . **Mahmoud Alneasan:** Writing – review & editing, Writing – original draft, Visualization, Validation, Software, Resources, Methodology, Investigation, Formal analysis, Data curation, Conceptualization. **Farid Ibrahim:** Writing – review & editing, Writing – original draft. **Nader M. Okasha:** Writing – review & editing, Writing – original draft. **Masoomeh Mirrashid:** Writing – review & editing, Writing – original draft.

Declaration of competing interest

The authors declare that they have no known competing financial interests or personal relationships that could have appeared to influence the work reported in this paper.

Data availability

Data will be made available on request.

Acknowledgment

We would like to thank the ORSP at Abu Dhabi University for funding this project (19300751, 19300798).

Appendix A

$$A_1 = \frac{1}{16\pi G}[(k - \cos\theta)(1 + \cos\theta)]$$

$$A_2 = \frac{1}{16\pi G}[k(1 - \cos\theta) + \cos\theta(1 + 3\cos\theta)]$$

$$A_3 = \frac{1}{16\pi G}[\sin\theta(2\cos\theta - (k - 1))]$$

$$A_4 = \frac{1}{16\pi G}\cos\frac{\theta}{2}[\cos 2\theta - \cos\theta + (k - 1)]$$

$$A_5 = \frac{-1}{16\pi G}\sin\frac{\theta}{2}[\cos 2\theta + \cos\theta + (k + 1)]$$

$$A_6 = \frac{1}{16\pi G}\left(\frac{k + 1}{2}\right)$$

$$C_1 = \frac{1}{16\pi G}\sin\theta_m[2\cos\theta_m - k + 1]$$

$$C_2 = \frac{-1}{16\pi G}\sin\theta_m[6\cos\theta_m - k + 1]$$

$$C_3 = \frac{1}{8\pi G}[2\cos 2\theta_m - (k - 1)\cos\theta_m]$$

$$C_4 = \frac{-1}{16\pi G}\sin\frac{\theta_m}{2}[5(\cos 2\theta_m + \cos\theta_m) + (k + 1)]$$

$$C_5 = \frac{-1}{16\pi G}\cos\frac{\theta_m}{2}[5(\cos 2\theta_m - \cos\theta_m) + (k + 3)]$$

$$C_5 = 0.0$$

$$D_1 = \frac{1}{4}\left[(8k - 5)\cos\frac{\theta}{2} + \cos\frac{3\theta}{2}\right]$$

$$D_2 = -\frac{1}{4}\left[(8k - 5)\sin\frac{\theta}{2} + 3\sin\frac{3\theta}{2}\right]$$

$$D_3 = k - \cos^2\theta$$

$$E_1 = -\frac{1}{8}\left[(8k - 5)\sin\frac{\theta_m}{2} + 3\sin\frac{3\theta_m}{2}\right]$$

$$E_2 = -\frac{1}{8}\left[(8k - 5)\cos\frac{\theta_m}{2} + 9\cos\frac{3\theta_m}{2}\right]$$

$$E_3 = \sin 2\theta_m$$

References

[1] H. Sun, et al., Temperature effect on microstructure and P-wave propagation in Linyi sandstone, Appl. Therm. Eng. 115 (2017) 913–922.
[2] S. Ge, et al., Thermal damage of high-temperature sandstone subjected to cooling shock and its effect on capturing acoustic emission signals during fracture, Eng. Fail. Anal. 145 (2023) 107003.
[3] X. Chen, et al., Mechanical-characteristic evaluation of excavation unloading rock mass subject to high-temperature conditions, Eng. Fail. Anal. 130 (2021) 105757.
[4] H.r. Karimi, et al., A comprehensive study on ring shape specimens under compressive and tensile loadings for covering the full range of I+II fracture modes of gypsum material, Int. J. Rock Mech. Min. 160 (2022) 105265.
[5] N.A. Al-Shayea, Crack propagation trajectories for rocks under mixed mode I-II fracture, Eng. Geol. 81 (1) (2005) 84–97.
[6] A.N. Poliakov, et al., Dynamic shear rupture interactions with fault bends and off-axis secondary faulting, J. Geophys. Res. Solid. 107(B11) (2002) ESE 6-1-ESE 6-18.
[7] B. Dehghani, L. Faramarzi, Experimental investigations of fracture toughness and crack initiation in marble under different freezing and thermal cyclic loading, Constr Build Mater. 220 (2019) 340–352.
[8] H. Meng, et al., A new insight into casing shear failure induced by natural fracture and artificial fracture slip, Eng. Fail. Anal. 137 (2022) 106287.
[9] F. Erdogan, G. Sih, On the crack extension in plates under plane loading and transverse shear, (1963).
[10] G.C. Sih, Strain-energy-density factor applied to mixed mode crack problems, Int. J. Fract. 10 (3) (1974) 305–321.
[11] C. Kaung Jain, On the maximum strain criterion—a new approach to the angled crack problem, Eng. Fract. Mech. 14 (1) (1981) 107–124.
[12] T. Meng, et al., Mixed mode fracture tests and inversion of FPZ at crack tip of overlying strata in underground coal gasification combustion cavity under real-time high temperature condition, Eng. Fract. Mech. 239 (2020) 107298.
[13] J.-P. Zuo, et al., Three-point bending test investigation of the fracture behavior of siltstone after thermal treatment, Int. J. Rock Mech. Min. 70 (2014) 133–143.
[14] B. Mahanta, et al., Influence of thermal treatment on mode I fracture toughness of certain Indian rocks, Eng. Geol. 210 (2016) 103–114.
[15] Q. Guo, et al., An experimental study on the fracture behaviors of marble specimens subjected to high temperature treatment, Eng. Fract. Mech. 225 (2020) 106862.
[16] K. Peng, et al., Evolutionary characteristics of mode-I fracture toughness and fracture energy in granite from different burial depths under high-temperature effect, Eng. Fract. Mech. 239 (2020) 107306.
[17] T.Y. Guo, et al., Microcracking behavior transition in thermally treated granite under mode I loading, Eng. Geol. 282 (2021) 105992.
[18] Y. Wu, et al., Determination of the mixed mode I/II fracture characteristics of heat-treated granite specimens based on the extended finite element method, Eng. Fract. Mech. 252 (2021) 107818.
[19] G. Feng, et al., The influence of temperatures on mixed-mode (I+II) and mode-II fracture toughness of sandstone, Eng. Fract. Mech. 189 (2018) 51–63.
[20] P. Kang, et al., Effects of temperature on mechanical properties of granite under different fracture modes, Eng. Fract. Mech. 226 (2020) 106838.
[21] T. Yin, et al., Mixed-mode I+ II tensile fracture analysis of thermally treated granite using straight-through notch Brazilian disc specimens, Eng. Fract. Mech. 234 (2020) 107111.
[22] G. Feng, et al., Experimental investigation of thermal cycling effect on fracture characteristics of granite in a geothermal-energy reservoir, Eng. Fract. Mech. 235 (2020) 107180.
[23] Y. Feng, et al., Mixed mode I-II fracture mechanism of sandstone samples after thermal treatment: Insights from optical monitoring and thermal analysis, Theor. Appl. Fract. Mech. 125 (2023) 103883.
[24] Y. Suo, et al., Mixed-mode fracture behavior in deep shale reservoirs under different loading rates and temperatures, Pet. Sci. (2023).
[25] M.-D. Wei, et al., Fracture prediction of rocks under mode I and mode II loading using the generalized maximum tangential strain criterion, Eng. Fract. Mech. 186 (2017) 21–38.
[26] D. Smith, et al., The role of T-stress in brittle fracture for linear elastic materials under mixed-mode loading, Fatigue Fract. Eng. Mater. Struct. 24 (2) (2001) 137–150.
[27] M. Ayatollahi, et al., A generalized strain energy density criterion for mixed mode fracture analysis in brittle and quasi-brittle materials, Theor. Appl. Fract. Mech. 79 (2015) 70–76.
[28] M.M. Mirsayar, Mixed mode fracture analysis using extended maximum tangential strain criterion, Mater. Des. 86 (2015) 941–947.
[29] M. Alneasan, M. Behnia, Analytical investigation on the effect of friction coefficient and crack inclination angle on the effective elastic properties and strength of brittle rocks, Innovative Infrastructure Solutions 7 (5) (2022) 1–11.
[30] S. Fliss, et al., Fault branching and rupture directivity, J. Geophys. Res. Solid. 110 (B6) (2005).
[31] W. Hua, et al., A review of mixed mode I-II fracture criteria and their applications in brittle or quasi-brittle fracture analysis, Theor. Appl. Fract. Mech. 124 (2023) 103741.
[32] G. Feng, et al., Thermal effects on prediction accuracy of dense granite mechanical behaviors using modified maximum tangential stress criterion, J. Rock Mech. Geotech. Eng. 15 (7) (2023) 1734–1748.
[33] J. Justo, J. Castro, Mechanical properties of 4 rocks at different temperatures and fracture assessment using the strain energy density criterion, Geomech. Energy Environ. 25 (2021) 100212.
[34] B.N. Whittaker, et al., Rock fracture mechanics, Principles, Design and Applications (1992).
[35] M.L. Williams, On the stress distribution at the base of a stationary crack, (1957).
[36] M.M. Mirsayar, et al., EMTSN criterion for evaluating mixed mode I/II crack propagation in rock materials, Eng. Fract. Mech. 190 (2018) 186–197.
[37] W. Hua, et al., Mixed mode fracture analysis of CCBD specimens based on the extended maximum tangential strain criterion, Fatigue Fract. Eng. Mater. Struct. 40 (12) (2017) 2118–2127.
[38] H. Gercek, Poisson's ratio values for rocks, Int. J. Rock Mech. Min. 44 (1) (2007) 1–13.
[39] N. Li, et al., Feasibility study on application of volume acid fracturing technology to tight gas carbonate reservoir development, Petroleum 1 (3) (2015) 206–216.
[40] T.-F. Wong, P. Baud, The brittle-ductile transition in porous rock: A review, J. Struct. Geol. 44 (2012) 25–53.
[41] M. Wei, F. Dai, Laboratory-scale mixed-mode I/II fracture tests on columnar saline ice, Theor. Appl. Fract. Mech. 114 (2021) 102982.
[42] W. Wang, et al., Assessment of thermal effect on the fracture toughness of granite, Theor. Appl. Fract. Mech. 122 (2022) 103575.
[43] X. Liu, et al., Effect of high temperature on mineralogy, microstructure, shear stiffness and tensile strength of two Australian mudstones, Rock Mech Rock Eng. 49 (2016) 3513–3524.
[44] M. Alneasan, A.K. Alzo'ubi, Comprehensive investigation of rock fracture behaviour in clay-rich rocks under the effect of temperature: Experimental study under three loading modes (I, I/II, II), Eng. Fract. Mech. 276 (2022) 108933.
[45] M. Alneasan, A.K. Alzo'ubi, Temperature Effect on the Fracture Behavior of Granite Under Three Loading Modes (I, I/II, and II), Rock Mech Rock Eng. (2022) 1-15.

[46] R.E. Goodman, Introduction to rock mechanics, John Wiley & Sons, 1991.
[47] T. Yin, et al., A numerical estimate method of dynamic fracture initiation toughness of rock under high temperature, Eng. Fract. Mech. 204 (2018) 87–102.
[48] W. Zhang, et al., Experimental study on mechanical and porous characteristics of limestone affected by high temperature, Appl. Therm. Eng. 110 (2017) 356–362.
[49] F. Meng, et al., Characterization of roughness and shear behavior of thermally treated granite fractures, Eng. Geol. 293 (2021) 106287.
[50] H. Fraser, Ceramic faults and their remedies, 1986.
[51] L. Griffiths, et al., Quantification of microcrack characteristics and implications for stiffness and strength of granite, Int. J. Rock Mech. Min. 100 (2017) 138–150.
[52] M.H.B. Nasseri, et al., Coupled evolutions of fracture toughness and elastic wave velocities at high crack density in thermally treated Westerly granite, Int. J. Rock Mech. Min. 44 (4) (2007) 601–616.
[53] B. Johnson, et al., Thermal cracking of rock subjected to slow, uniform temperature changes, ARMA US Rock Mechanics/Geomechanics Symposium, ARMA (1978) pp. ARMA-78-0318.
[54] M.J. Trindade, et al., Mineralogical transformations of calcareous rich clays with firing: a comparative study between calcite and dolomite rich clays from Algarve, Portugal, Applied Clay Science 42 (3–4) (2009) 345–355.
[55] K. Liu, et al., Dynamic increase factors of rock strength, Proceedings of the Third International Confrence on Rock Dynamics and Applications, Trondheim, 26-27 June (2018) 169-174.
[56] T. Yin, et al., Determination of double-K fracture toughness parameters of thermally treated granite using notched semi-circular bending specimen, Eng. Fract. Mech. 226 (2020) 106865.
[57] M.R.M. Aliha, et al., Typical Upper Bound-Lower Bound Mixed Mode Fracture Resistance Envelopes for Rock Material, Rock Mech Rock Eng. 45 (1) (2012) 65–74.
[58] M.R. Ayatollahi, M.R.M. Aliha, Mixed mode fracture in soda lime glass analyzed by using the generalized MTS criterion, Int J Solids Struct. 46 (2) (2009) 311–321.
[59] R.A. Schmidt, A. Microcrack, Model and Its Significance to Hydraulic Fracturing and Fracture Toughness Testing, the, 1980.
[60] B. Xiankai, et al., Study of mixed mode fracture toughness and fracture trajectories in gypsum interlayers in corrosive environment, R. Soc. Open Sci. 5 (1) (2018) 171374.
[61] T. Meng, et al., Study of mixed mode fracture toughness and fracture characteristic in gypsum rock under brine saturation, Environ. Earth Sci. 77 (2018) 1–25.
[62] M. Wei, et al., A fracture model for assessing tensile mode crack growth resistance of rocks, J. Rock Mech. Geotech. Eng. 15 (2) (2023) 395–411.
[63] G. Feng, et al., Effect of thermal cycling-dependent cracks on physical and mechanical properties of granite for enhanced geothermal system, Int. J. Rock Mech. Min. 134 (2020) 104476.
[64] S. Kou, Effect of thermal cracking damage on the deformation and failure of granite, Acta Mechanica Sinica 19 (6) (1987) 550–556.
[65] Z.-X. Zhang, et al., The relationship between the fracture toughness and tensile strength of rock, Strength theories, in: Applications, Development & Prospects for 21st Century, 1998, pp. 215–219.
[66] Z.X. Zhang, An empirical relation between mode I fracture toughness and the tensile strength of rock, Int. J. Rock Mech. Min. 39 (3) (2002) 401–406.
[67] G. Wang, Experiment research on the effects of temperature and viscoelastoplastic analysis of Beishan granite, Xi'an University of Science and Technology, 2003.
[68] G. Feng, et al., Effects of temperature on the relationship between mode-I fracture toughness and tensile strength of rock, Appl. Sci. 9 (7) (2019) 1326.
[69] A. Tarokh, et al., Evaluation of brittleness from spalling and bending tests, ARMA US Rock Mechanics/Geomechanics Symposium, ARMA (2016) pp. ARMA-2016-800.
[70] P. Meredith, B. Atkinson, Fracture toughness and subcritical crack growth during high-temperature tensile deformation of Westerly granite and Black gabbro, Phys. Earth Planet. in. 39 (1) (1985) 33–51.
[71] H. Su, et al., Experimental investigation of mixed mode I-II fracture property of thermally treated granite under dynamic loading, Theor. Appl. Fract. Mech. 118 (2022) 103267.
[72] T. Yin, et al., Effect of thermal treatment on the dynamic fracture toughness of Laurentian granite, Rock Mech Rock Eng. 45 (6) (2012) 1087–1094.
[73] A.K. Alzo'ubi, M. Alneasan, Experimental study on the effect of thermal treatment on the mechanical properties of clay-rich rocks (mudstone), Results Eng. (2022) 100728.
[74] M. Alneasan, et al., Experimental Observations on The Effect of Thermal Treatment on the Crack Speed and Mode I and II Fracture toughness in brittle and ductile rocks, Theor. Appl. Fract. Mech. 103525 (2022).